Model-free Phasor Image Analysis of Quantitative Myocardial T_1 Mapping

Wouter M. J. Franssen
Wageningen University & Research
Thomas A. Treibel
University College London
Andreas Seraphim
University College London
Sebastian Weingärtner
Delft University of Technology
Camilla Terenzi (camilla.terenzi@wur.nl)
Wageningen University & Research

Research Article

Keywords: qMRI, Myocardium, Phasor, T1 mapping, Partial-volume, Motion, Coronary heart disease

Posted Date: February 25th, 2022

DOI: https://doi.org/10.21203/rs.3.rs-1335386/v1

Abstract

Model-free phasor image analysis, well established in fluorescence lifetime imaging and only recently applied to qMRI T_2 data processing, is here adapted and validated for myocardial qMRI T_1 mapping. Contrarily to routine mono-exponential fitting procedures, phasor enables mapping the lifetime information from all image voxels to a single plot, without resorting to any regression fit analysis, and describing multi-exponential qMRI decays without biases due to violated modelling assumptions. In this study, we test the performance of our recently developed full-harmonics phasor method for unravelling partial-volume effects, motion or pathological tissue alteration, respectively on a numerically-simulated dataset, a healthy subject scan, and two pilot patient datasets. Our results show that phasor analysis can be used, as alternative method to fitting analysis or other model-free approaches, to identify motion artifacts or partial-volume effects at the myocardium-blood interface as characteristic deviations, or delineations of scar and remote myocardial tissue in patient data.

1 Introduction

Quantitative Magnetic Resonance Imaging (qMRI) has emerged as a promising tool for myocardial tissue characterization with a growing number of clinical applications[1]. Localized or global changes in relaxation time parameters (T_1, T_2, T_2^*) have been shown to be useful clinical markers, specifically for focal or diffuse pathological tissue alterations in the myocardium.[2–4] Thus, relaxation time mapping, *i.e.* the voxel-wise quantification of relaxation times, is increasingly more established in clinical use.[2]

Native myocardial T_1 mapping is most commonly used in cardiovascular MRI, and a recommended part of the clinical work-up for a number of disease entities, including amyloidosis, Anderson-Fabry disease and myocarditis.[2, 5–7] Modified Look-Locker Inversion Recovery (MOLLI)[8] is most commonly used for cardiac T_1 measurements, and enables sampling the Inversion Recovery curve in a single breath-hold. For MOLLI data, mono-exponential fitting is conventionally used to obtain T_1 maps, although it is well known that qMRI data with either multi- or non-exponential character may be incorrectly described.[9,10] Yet, bi-exponential fitting typically leads to large processing errors when applied to data with limited signal-to-noise ratio (SNR) such as clinical T_1 maps.

Furthermore, data corruption induced by, *e.g.*, motion may lead to a large deviation from the fitting model, resulting in non-robust results.[11,12] Multiple techniques for motion correction have previously been proposed.[11–14] However, it has been suggested that identifying motion during the scan and reacquiring the maps, if needed, is a more effective way to overcome motion challenges.[15] To this end robust and versatile methods of motion detection are highly desirable.

In this work, we explore the performance of a robust, fitting-free, lifetime image processing method, called phasor analysis, for unravelling partial-volume effects, motion or pathological tissue alteration in myocardial T_1 qMRI data. Phasor method was originally developed for, and is nowadays routinely used

in, fluorescence lifetime imaging (FLIM) studies.[16] Very recently this method has been adapted[17], and further optimized by some of us[18], for the analysis of T_2 and diffusion qMRI relaxometry data from a range of systems, including bio-medical tissues.[19] Phasor relies on the mathematically-exact Fourier Transform (FT) analysis of all the measured signal decays within the image and, thus, provides information about the distribution of lifetimes across the voxels without resorting to fitting procedures. In conventional phasor analysis, only the first or second Fourier coefficient are typically used, *e.g.* in FLIM studies, as they contain the highest signal intensity. The real and imaginary parts of such Fourier coefficients are then displayed in a two-dimensional graph called 'phasor plot' for all image voxels simultaneously.[16] Such phasor plot enables straightforward identification of signal decays for all image voxels. Mono-exponential behaviours are readily identified by the clustering of datapoints along a reference semicircle curve. Datapoints in the phasor plot, which lie below this reference mono-exponential curve, refer to voxels with multi-exponentially decaying signals. Hence, the distribution of such datapoints is key to unravelling the number of exponential terms present in the signal decays across the image. In our recently developed full-harmonics approach, where all Fourier coefficients are retained for constructing the phasor plot, the unmixing accuracy of phasor analysis for data with multi-modal decays was shown to be maximized.[18] This improvement turned out crucial for boosting the ability of phasor representation to unravel *inter*-voxel trends across the image such as, *e.g.*, partial-volume effects. In phasor analysis, all the above-mentioned information is achieved without introducing any fitting error or model assumption, and can be exploited as prior knowledge for any subsequent image analysis step, iterative or non. For instance, we have shown that phasor-coordinate images can be reconstructed and yield consistent information as compared to qMRI relaxation maps obtained by fitting analysis.[18]

In this paper, we evaluate the use of full-harmonics phasor processing for the analysis of cardiac T_1 mapping data, and for the first time we apply this method to the identification of motion corruption and of pathological tissue alterations. To these scopes, in analogy to the approach adopted for characterizing partial-volume effects[18], we exploit both phasor-coordinate images, to be directly compared with T_1 maps, and phasor plot representations, where deviations from neat uni- or multi-modal signal decay behaviours are readily identified. First, numerically simulated data are used to explore the effect of partial-voluming and motion-corruption in phasor analysis. Secondly, cardiac T_1 mapping data from healthy subjects are used to validate such phasor characterization *in-vivo*. Finally, pilot patient phasor data are obtained to evaluate the ability of our proposed image analysis method to discern diseased myocardial tissue.

2 Materials And Methods

2.1 Phasor processing

Phasor processing of qMRI relaxation data can be used to map the signal decay from each image voxel to a lifetime value on a 2D phasor plane. Such conversion is obtained, per voxel, by the FT of the respective measured decay along the sampled contrast dimension, *e.g.* given by the number of echoes in

T_2 mapping or by the inversion time (TI) in T_1 mapping. As explained in detail elsewhere,[16,18] all datapoints in each FT curve of the image are normalized to the respective real value of the zeroth-order Fourier coefficient of the FT dataset. The latter value in turn corresponds to the measured equilibrium ^{1}H NMR signal intensity, or integral area of the measured signal decay over the contrast dimension. The set of sampled Fourier coefficients, with their real and imaginary parts, can be used to define two suitable variables that are plotted against each other in the phasor plot. Traditionally, only the real and imaginary parts of the first Fourier harmonic, here respectively denoted as Re_1 and Im_1, are used in FLIM phasor studies.[16] We have recently shown that a more accurate mapping of the phasor-space information to a 2D plot is achieved when using all Fourier coefficients, or 'harmonics', simultaneously.[18] This approach requires handling $N-$ dimensional phasor-space data, where N is the number of measured Fourier harmonics, and hence defining a two-dimensional projection phasor plane based on the selection of three lifetimes. The full-harmonics phasor algorithm, also used in the present work, has been already described in detail and successfully validated elsewhere.[18]

The specific position of a point in the phasor plot depends on the lifetime and multi-modal character of the corresponding signal decay function. Because the phasor coordinates of all voxels in the imaging dataset are plotted simultaneously, voxels with similar relaxation decay properties will lead to clusters of data points. Distinguishing such clusters is key to enabling the identification of different tissues, with distinct lifetimes, in a model- and fitting-free way.

In order to get a handhold of this, a reference curve, also called 'semicircle', is generally displayed within the phasor plot. This reference curve is obtained by plotting the phasor coordinates of image voxels whose signal decays are single-exponential decays, with lifetimes chosen over a range wide enough to represent the measured data. In such phasor representation, image voxels whose phasor coordinates lie along the reference curve are unequivocally described by a mono-exponential decay. In general, image voxels with multi-exponential decays fall below the phasor reference semicircle, while those with non-exponential, *e.g.* gaussian, decay functions fall above such reference curve. A useful property of the phasor plot representation is that image voxels with bi-exponential signal decays yield points that fall along a straight line connecting the phasor coordinates, along the semicircle, of the two respective lifetimes. This is the case of image voxels with partial-volume effects, *i.e.* containing overlapping signals from two distinct tissue types. Datapoints from such voxels appear continuously distributed along a line below the semicircle, as a consequence of the varying signal intensity ratios between the two tissues. As described elsewhere[17,18], three- or four-exponential decays respectively lead to triangular- or rectangular-shaped clouds of phasor-space coordinate values.

Conventional phasor processing, as adopted in FLIM, requires the imaging signal to decay as a function of a contrast parameter. In qMRI measurements, this occurs in the case of both T_2 relaxation and diffusion data. Indeed, these types of qMRI data have already been successfully investigated by phasor.[17–19] In the present work, we set out to validate the use of phasor also for Inversion Recovery T_1 data, where signal intensities instead follow an exponentially increasing function. For the purpose of

phasor analysis, such type of data must be re-shaped in order to obtain time-decaying behaviours. This can be achieved, as done in the present work, by flipping the sign of the whole measured dataset, and then subtracting, per voxel, the respective signal intensity value at the longest inversion time. This leads to signal intensity data which decay exponentially towards zero, similarly to a T_2 relaxation decay. This adjusted qMRI T_1 dataset can then be processed by phasor. If the mono-exponential reference curve is reconstructed in this way, all the above-mentioned useful characteristics of a phasor plot are retained.[10,11]

2.2 Numerical simulations

A numerical phantom of the myocardium was created to resemble the left ventricle in short-axis view, by simulating two exponential signal decays for two distinct areas, namely: an outer ring, mimicking the myocardial tissue, and its inner circular area, corresponding to the signal from blood. The signal intensity for voxels outside the simulated phantom was fixed to zero. The equilibrium value of the ^{1}H MRI signal intensity per unit volume was normalized to 1 for both myocardium and blood regions. Using this definition, a 1000x1000 grid of voxels was generated and subsequently down-sized to a 21x21 grid to simulate partial-volume effects. For each voxel within the down-sized data, with known myocardium and blood signal intensities, a bi-exponential signal decay was simulated using T_1 values of 1500 and 2000 ms for myocardium and blood, respectively. The sampled time points were 129, 209, 1344, 1394, 2494, 2551, 3644, and 4807 ms, for comparison with the measured dataset discussed in Section 3.3.1. An offset correction was performed, as described in Section 2.1. The full-harmonics phasor projection plane was defined by using three T_1 values, namely 1.5, 1.75, and 2 s.

The position of data points in the phasor plot can be converted to a myocardium volume fraction by comparing the observed position with a pre-calculated library of positions for all possible volume fractions, using these specific T_1 values for blood and myocardium muscle respectively. The S_{myo}/S_{tot} value that, in the phasor plot, lies closest to the experimental point is then selected as the S_{myo}/S_{tot} value for this experimental point.

Segmentation of the imaging data into three distinct areas, namely myocardium, blood, and regions with partial-volume effects, was obtained by using the $x-$ coordinate of the phasor plot, namely $Axis1$, respectively using $0.88 > Axis1 > 0.85$ for myocardium, $0.85 > Axis1 > 0.43$ for partial-volume voxels, and $0.43 > Axis1 > 0.41$ for blood.

2.3 Healthy subjects

Patients and controls were recruited under ethics approved by the ethical committee of UK National Research Ethics Service (07/H0715/101), conforming to the principles of the Helsinki Declaration, and all subjects gave written informed consent.

2.3.1 Partial-volume effects

Healthy subject data was acquired for one volunteer (male, 28 years old) using the MOLLI pulse sequence[8] on a 3T MRI scanner (Magnetom Skyra; Siemens Healthineers, Erlangen, Germany) with the following imaging parameters: balanced Steady-State Free-Precession image acquisition (bSSFP); TR/TE/α = 2.6 ms/1.0 ms/35°, in-plane resolution = 1.7 × 1.7 mm^2, slice-thickness = 6 mm, field-of-view = 440 × 375 mm^2, bandwidth = 1085 Hz/px, number of k-space lines = 139, linear profile ordering, startup-pulses = 5 Kaiser-Bessel, GRAPPA-factor = 2. The 5(3s)3 MOLLI scheme was employed for native T_1-mapping.

Regions-of-interest (ROIs) for phasor analysis were assigned based on the last intensity image of the series, and the myocardium ring and the voxels within this were selected.

2.3.2 Measured and simulated motion-corruption effects

A second set of healthy subject data was acquired on a 26 years old man using MOLLI on a 3T MRI scanner (Ingenia; Philips, Best, Netherlands). The following imaging parameters were used: balanced Steady-State Free-Precession image acquisition (bSSFP); TR/TE/α = 2.3 ms/1.1 ms/20°, in-plane resolution = 2.0 × 2.0 mm^2, slice-thickness = 8 mm, field-of-view = 280 × 280 mm^2, bandwidth = 1082 Hz/px, number of k-space lines = 90, linear profile ordering, startup-pulses = 10 linear sweep-up, SENSE-factor = 2. The 5s(3s)3s MOLLI scheme was employed for native T_1-mapping. Data were acquired either during breath-holding or during free-breathing, in order to study the effect of respiratory-induced motion artifacts.

In order to mimic a sudden movement between subsequent signal acquisitions with the MOLLI sequence, simulated motion was artificially added to the breath-hold measured dataset by shifting along the vertical spatial direction, by 8 voxels (9.3 mm), the voxels in the MRI images corresponding to the even-numbered inversion time values. As a region-of-interest (ROI), the ring of myocardium tissue and its inner region were selected based on the image corresponding to the fourth inversion time, namely 1213 ms. This image was selected for its highest visual contrast between myocardium and blood, and the definition of the ROI is shown in Figure S1 of SI. The selected ROI was symmetrically broadened by 10 pixels along all directions, to accommodate also all motion-shifted voxels.

2.4 Patients

Patient data were acquired in two subjects with obstructive coronary artery disease and evidence of myocardial infarction (57 and 76 years old, both male). Patient imaging was performed at 1.5T (Magnetom Aera; Siemens Healthineers, Erlangen, Germany). Identical image parameters to the subjects in 2.3.1 were used except for the following: TR/TE/α = 2.6 ms/1.1 ms/35°, in-plane resolution = 1.7 × 1.7 mm^2, slice-thickness = 8 mm, field-of-view = 430 × 322 mm^2, bandwidth = 1085 Hz/px, number of k — space lines = 125, linear profile ordering, startup-pulses = Kaiser-Bessel, GRAPPA-factor = 2, 5(3s)3 MOLLI scheme. Additionally, conventional 2D PSIR Late Gadolinium Enhanced (LGE) Images were acquired for reference.

The ROIs for phasor analysis were assigned based on the image acquired at the longest inversion time, namely 4807 ms, and are shown in Figure S2 of SI alongside the respective labelling of healthy and scarred tissues.

3 Results

3.1 Numerical simulation of cardiac T_1 data

We first demonstrate the validity of our full-harmonics phasor processing method on a virtual heart phantom, schematically depicted in Fig. 1a, for which T_1 mapping data were numerically simulated. This phantom was designed to contain voxels with individual T_1 values from either blood (red) or myocardium (blue), as well as voxels containing both compartments.

Figures 1b shows the resulting phasor plot for this simulated dataset obtained by using the full-harmonics method.[18] The data points (filled black circles) from all voxels in Fig. 1a fall along a straight line connecting two points (filled green circles) along the reference phasor curve (solid green line). Such phasor-space points, correspond to the T_1 values for myocardium (rightmost point) and blood (leftmost point) ^{1}H signals, respectively. Data points distributed continuously along the straight line connecting these two points represent all voxels in the simulated qMRI dataset that contain *both* blood and myocardial ^{1}H T_1 values, in varying relative fractions of tissue and blood.

The existence of voxels with signal from both myocardium and blood can be directly visualized by reconstructing an image of the virtual heart phantom using, as contrast intensity scale, the corresponding phasor-space coordinate, $Axis1$, in Fig. 1b. Such phasor-space coordinate corresponds to the myocardium volume percentage S_{myo} / S_{tot} (see Section 2.2). In this phasor-based image (Fig. 1c), voxels which contain both myocardial and blood compartments are coloured in-between. From such an image, a segmentation map can be obtained (Fig. 1d) where the net blood (white) or tissue (dark grey) environments are clearly distinguished from voxels containing both compartments (light gray).

3.2 Healthy subjects: partial-volume or motion-corruption effects

Figure 2 demonstrates the result of full-harmonics phasor analysis on MOLLI T_1 data acquired on a healthy individual. Figure 2a shows the MRI image acquired at the longest inversion time, extracted from the T_1 data, where the ROI selected for further phasor analysis is highlighted. In the phasor plot of such data (Fig. 2b), the blood (left) and myocardium (right) signal clusters are connected by a straight band of data points that lies below the mono-exponential reference phasor curve, in analogy with what observed for the simulated hearth phantom (Fig. 1b). The larger data dispersion around the straight line, as compared to the numerical simulation results shown in Fig. 1b, is due both to the presence of noise, not included in the simulations of Section 3.1, and to the larger structural heterogeneity in the measured cardiac data.

Figures 2c shows the T_1 map obtained by single-exponential two-parameter fitting of the data. Figures 2d and 2e respectively show the phasor-coordinate map and its corresponding segmentation results. In analogy to Figure 1d for the simulated phantom, Figure 2e enables spatially identifying voxels (light grey) with co-existence of blood (white) and myocardial (dark grey) T_1 components.

In Fig. 3a demonstration is shown of the performance of phasor analysis for the investigation of motion-induced corruption artifacts in T_1 mapping images. To this scope, phasor plots and T_1 maps for data acquired on a healthy volunteer in the absence of motion artifacts (Figs. 3a and 3d) are compared with the results obtained either from the same dataset, by artefactually shifting the image voxels as described in section 2.3.2 (Figs. 3b and 3e), or from data acquired, on the same healthy volunteer, under free-breathing conditions (Figs. 3c and 3f). In the phasor plots, the presence of motion artifacts is detected as an increase in the scatter of the data points along the direction perpendicular to the single-exponential reference phasor curve.

3.3 Patients: identification of scarred myocardial tissue

To further illustrate the applicability of phasor processing to the analysis of T_1 mapping data of myocardium, we have examined the images from two different diseased patients. Both patients exhibit sub-endocardial scarring. Figure 4 shows the comparison of the hyperintense scar areas in LGE images (Figs. 4a and 4e) with the corresponding T_1 (Figs. 4b and 4f) or phasor-coordinates (Figs. 4c and 4g) images. In the latter two images, two ROIs are marked with an arrow: namely, an area of normal myocardium (blue) and that for the scarred tissue (red). In the respective phasor plots (Figs. 4d and 4h), on top of the whole set of data points corresponding to the phasor-coordinate images (grey filled circles), also the datapoints corresponding solely to either the normal (blue filled circles) or the scarred (red filled circles) tissue are highlighted.

4 Discussion

This work aimed at showing the performance of phasor analysis as alternative non-fitting qMRI image processing method for applications to T_1 mapping data from healthy or diseased myocardial tissues. To this end, we have targeted (i) the identification of partial-volume effects and motion-induced artifacts in cardiac T_1 data in the absence of a disease, and (ii) the delineation of pathological tissue in pilot patient data. We have tested a recently introduced full-harmonics phasor analysis, which has been validated for the characterization of multi-exponential T_2 qMRI decays.[17,18] This method has been shown to maximize the unmixing accuracy as compared to conventional, single-harmonics, phasor analysis. In this work, our optimized full-harmonics phasor processing approach has been further adjusted for the analysis of T_1 qMRI datasets, by introducing baseline correction and sign adjustment in order to transform the acquired dataset into a signal decay similar to that of T_2 relaxation. As discussed in section 2.1, this data conversion step is needed in order to apply the FT analysis and obtain the phasor plots.

Our first demonstration in Fig. 1 concerned numerically simulated T_1 data for a virtual myocardium phantom, containing voxels with blood or myocardial tissue only, as well as voxels with both components. Full-harmonics phasor plots indicate that there are two clusters of voxels with mono-exponential T_1 character, which fall along the phasor reference curve. These clusters of voxels correspond to the signal from either myocardium tissue or blood. In addition, there is a set of voxels at the interface between these two regions that exhibit partial-volume effects. These voxels yield phasor data points lying along a straight line that intersects the mono-exponential reference curve in correspondence of the lifetimes of myocardium or blood signal decays. The position of each voxel along such line depends on its specific myocardium-to-blood signal intensity ratio. We note that, in the absence of partial-volume effects, only two isolated clusters of data points would be observed, respectively centred around the phasor coordinates for either myocardium or blood individual lifetimes.

From the phasor plot in Fig. 1b, we have obtained an image of the phasor-space coordinates, indicative of the myocardium volume fraction. The latter image was further processed for reconstructing a segmented image based on phasor analysis (Fig. 2e). The same image analysis approach has been applied to analyse a T_1 mapping dataset collected from a healthy volunteer in the absence of motion artifacts (Fig. 2). Results are consistent with the simulations shown in Fig. 1. Also for the *in-vivo* data, the phasor plot in Fig. 2b shows clear evidence of partial-volume effects between myocardium and blood signal pools. We note that, as compared to the simulated data in Fig. 1b, for the real case study a wider scatter of data points around the straight line exists due to that in Fig. 2b both noise and structural heterogeneities are present. From this first validation of phasor analysis on both simulated and measured T_1 mapping data for a healthy myocardium, we conclude that our adjusted phasor processing method works correctly for T_1 qMRI build-up curves, in analogy to our recent demonstrations of the method for T_2 relaxation or diffusion maps.[17–19] Hence, phasor plots enable unmixing multiple relaxation components in cardiac T_1 qMRI data without the need to use a fitting procedure. In addition, phasor processing is shown to enable visually unravelling *inter*-voxel correlations in cardiac qMRI T_1 data, such as partial-volume effects, that cannot be detected by per-voxel fitting methods. For the purpose of identifying partial-volume effects, both phasor plots and segmented phasor-coordinate images can be successfully used.

After this initial validation on cardiac data in the absence of MRI artifacts or disease, we have investigated the effect of simulated and measured motion on a T_1 qMRI dataset acquired from a healthy volunteer (Fig. 3). For a MOLLI experiment, motion causes per-voxel distortions in the signal recovery curves, because in such case the signal per voxel at each inversion time point originates from a different position in the body. As illustrated in Figs. 1 and 2 and in our previous works,[17,18] phasor offers a convenient way to directly visualize, within a single plot, signal characteristics that arise from all voxels in the image. Hence, any motion artifact in the dataset is expected to yield a readily visible effect in the clustering of data points within the phasor plot. Indeed, the simulation results in Fig. 3b indicate that, with a simulated motion of about 9.3 mm, the scatter of datapoints around the straight line increases by a factor of about 1.5 as compared to the same data without an added motion-induced shift. Similarly, the

phasor plot in Fig. 3c shows an increased scatter of data points around the straight line by a factor of about 2. The associated T_1 maps show some loss of resolution, but no further indication of motion.

Our data indicates, that phasor can be a useful tool in identifying a motion fingerprint in qMRI acquisitions. Its short processing times allow for seamless integration in a clinical workflow, enabling the user to reacquire maps if motion artifacts are detected. This workflow has previously been proposed based on machine learning quality assurance[15]. However, a large database of training maps is required in the learning-based approach to robustly identify motion. Phasor is a learning-free method, that does not require reference databases, but motion can be detected from deviations of the expected decay model. Future research is warranted to investigate the clinical value of a phasor-based rapid motion quality assurance to aid robustness in clinical cardiac T_1 mapping.

We conclude that phasor representation, in the form of phasor plots and/or phasor-based images, is consistent with the information provided by single-exponential fitting, but in addition can aid the characterization of *inter*-voxel features and motion artifacts in T_1 qMRI data that cannot be easily, or at all in some cases, detected by visual inspection of conventional T_1 maps.

Based on the successful validation of phasor processing for T_1 qMRI data from healthy volunteers, we have applied the same image analysis approach to inspect similar data from two patients with scarred myocardial tissue. Results in Fig. 4 further confirm that T_1 maps and phasor-coordinates images show similar results, and demonstrate that the scarred tissue can be identified in both representations. Remarkably, the phasor plot indicates that voxels involving either normal or scarred myocardial tissue cluster around neatly distinct areas with respect to phasor coordinates, *i.e.* with respect to the myocardial volume fraction. Specifically, in the examined case of a scar whose size is appreciable in conventional LGE and T_1 maps, a cluster of data points shows up in the phasor plot, between the region interested by the healthy myocardium and that related to the blood pool. In a healthy myocardium, no such intermediate cluster of data points (in red in Fig. 4b) is detected. Hence, phasor plots can be used to readily identify, without resorting to any fitting procedure or assumption on number of exponential decays in T_1 qMRI data, the presence or absence of scarred myocardial tissue in T_1 images acquired without the use of contrast agents.

The phasor approach can be of special interest for cases where the mono-exponential model is by definition not applicable. Examples of these systems are quadrupolar nuclei, where both the T_1 and T_2 relaxation models are multiexponential by nature, or systems with susceptibility enclosures such as the lungs or the vicinity of blood vessels where the transverse magnetization decay has been shown to deviate from a mono-exponential decay.[20,21] Finally, due to the complex nature of biological tissue, the accuracy of the phenomenological Bloch equations in those systems has also been challenged under certain circumstances.[22,23] Thus, a model-free evaluation may generally yield additional insights especially if highly accurate measurement techniques are being used. Finally, the computational ease

and independence from fitting procedures of phasor can be utilized for the ever-increasing efforts towards optimizing the use of machine learning algorithms for the analysis of big qMRI data.

5 Conclusions

In this work, we have evaluated the feasibility of phasor processing method for the analysis of cardiac T_1 mapping data. Our data indicate the potential use of phasor analysis, in the form of both phasor-coordinate maps and phasor plots, for the eased depiction of partial volume effects and motion, while retaining good visualization of abnormal relaxation times in patients. Hence, phasor may offer potential as an alternative model-free qMRI data analysis method for fast and robust tissue characterization based on conventional myocardial T_1 mapping data.

Abbreviations

qMRI, quantitative MRI; MOLLI, Modified Look-Locker Inversion Recovery; FT, Fourier Transform; ROI, region-of-interest; LGE, Late Gadolinium Enhanced

Declarations

Acknowledgments

This work is part of the 4TU Precision Medicine program supported by High Tech for a Sustainable Future, a framework commissioned by the four Universities of Technology of the Netherlands (https://www.4tu.nl/en/news/!/393/awarding_hightech/). S.W. acknowledges funding by an NWO Start-Up Grant (STU.019.024), and ZonMW OffRoad (04510011910073).

Data availability

The datasets generated during the current study are available from the corresponding author on reasonable request. The description of the code used for full-harmonics phasor analysis is described in detail in our previous publication: https://pubs.acs.org/doi/pdf/10.1021/acs.jpclett.0c02319.

AUTHOR'S CONTRIBUTION

W.M.F. performed the simulations, analysed all data, wrote the phasor analysis code and the first draft of the manuscript. T-A.T. and A.S. consented, recruited and collected the healthy subject and patient data. S.W. contributed to results discussion and revised the manuscript. C.T. supervised the work and wrote the final version of the manuscript.

Competing interests

The authors declare no competing interests.

References

1. Taylor, A. J., Salerno, M., Dharmakumar, R. & Jerosch-Herold, M. T1 Mapping Basic Techniques and Clinical Applications. *JACC Cardiovasc. Imaging* **9**, 67-81, (2016).
2. Haaf, P. *et al.* Cardiac T1 Mapping and Extracellular Volume (ECV) in clinical practice: a comprehensive review. *J. Cardiovasc. Magn. Reson.* **18**, 89, (2016).
3. Hanson, C. A., Kamath, A., Gottbrecht, M., Ibrahim, S. & Salerno, M. T2 Relaxation Times at Cardiac MRI in Healthy Adults: A Systematic Review and Meta-Analysis. *Radiology* **297**, 344-351, (2020).
4. Triadyaksa, P., Oudkerk, M. & Sijens, P. E. Cardiac T-2* mapping: Techniques and clinical applications. *J. Magn. Reson. Imaging* **52**, 1340-1351, (2020).
5. Ferreira, V. M. *et al.* Cardiovascular Magnetic Resonance in Nonischemic Myocardial Inflammation Expert Recommendations. *J. Am. Coll. Cardiol.* **72**, 3158-3176, (2018).
6. Jellis, C. L. & Kwon, D. H. Myocardial T1 mapping: modalities and clinical applications. *Cardiovasc. Diagn. Ther.* **4**, 126-137, (2014).
7. Karamitsos, T. D. *et al.* Noncontrast T1 Mapping for the Diagnosis of Cardiac Amyloidosis. *JACC Cardiovasc. Imaging* **6**, 488-497, (2013).
8. Messroghli, D. R. *et al.* Modified Look-Locker inversion recovery (MOLLI) for high-resolution T1 mapping of the heart. *Magn. Reson. Med.* **52**, 141-146, (2004).
9. Cameron, D., Vassiliou, V. S., Higgins, D. M. & Gatehouse, P. D. Towards accurate and precise T (1) and extracellular volume mapping in the myocardium: a guide to current pitfalls and their solutions. *MAGMA* **31**, 143-163, (2018).
10. Weingärtner, S., Messner, N. M., Zollner, F. G., Akcakaya, M. & Schad, L. R. Black-blood native T-1 mapping: Blood signal suppression for reduced partial voluming in the myocardium. *Magn. Reson. Med.* **78**, 484-493, (2017).
11. Roujol, S., Foppa, M., Weingärtner, S., Manning, W. J. & Nezafat, R. Adaptive Registration of Varying Contrast-Weighted Images for Improved Tissue Characterization (ARCTIC): Application to T-1 Mapping. *Magn. Reson. Med.* **73**, 1469-1482, (2015).
12. Xue, H. *et al.* Motion correction for myocardial T1 mapping using image registration with synthetic image estimation. *Magn. Reson. Med.* **67**, 1644-1655, (2012).
13. Tao, Q. *et al.* Robust motion correction for myocardial T-1 and extracellular volume mapping by principle component analysis-based groupwise image registration. *Journal of Magnetic Resonance Imaging* **47**, 1397-1405, (2018).
14. Weingärtner, S. *et al.* Myocardial T-1-mapping at 3T using saturation-recovery: reference values, precision and comparison with MOLLI. *J. Cardiov. Magn. Reson.* **18**, 9, (2016).
15. Zhang, Q. *et al.* Deep learning with attention supervision for automated motion artefact detection in quality control of cardiac T1-mapping. *Artif. Intell. Med.* **110**, 9, (2020).
16. Digman, M. A., Caiolfa, V. R., Zamai, M. & Gratton, E. The phasor approach to fluorescence lifetime imaging analysis. *Biophys. J.* **94**, L14-16, (2008).

17. Vergeldt, F. J. *et al.* Multi-component quantitative magnetic resonance imaging by phasor representation. *Sci. Rep.* **7**, 861, (2017).
18. Franssen, W. M. J., Vergeldt, F. J., Bader, A. N., van Amerongen, H. & Terenzi, C. Full-Harmonics Phasor Analysis: Unravelling Multiexponential Trends in Magnetic Resonance Imaging Data. *J. Phys. Chem. Lett.* **11**, 9152-9158, (2020).
19. van Rijssel, M. J., Froeling, M., van Lier, A., Verhoeff, J. J. C. & Pluim, J. P. W. Untangling the diffusion signal using the phasor transform. *NMR Biomed.*, e4372, (2020).
20. Sedlacik, J., Rauscher, A. & Reichenbach, J. R. Obtaining blood oxygenation levels from MR signal behavior in the presence of single venous vessels. *Magn. Reson. Med.* **58**, 1035-1044, (2007).
21. Zapp, J., Domsch, S., Weingärtner, S. & Schad, L. R. Gaussian signal relaxation around spin echoes: Implications for precise reversible transverse relaxation quantification of pulmonary tissue at 1.5 and 3 Tesla. *Magn. Reson. Med.* **77**, 1938-1945, (2017).
22. Magin, R. L. *et al.* Anomalous NMR relaxation in cartilage matrix components and native cartilage: Fractional-order models. *J. Magn. Reson.* **210**, 184-191, (2011).
23. Qin, S. L. *et al.* Characterization of Anomalous Relaxation Using the Time-Fractional Bloch Equation and Multiple Echo T-2(*)-Weighted Magnetic Resonance Imaging at 7 T. *Magn. Reson. Med.* **77**, 1485-1494, (2017).

Figures

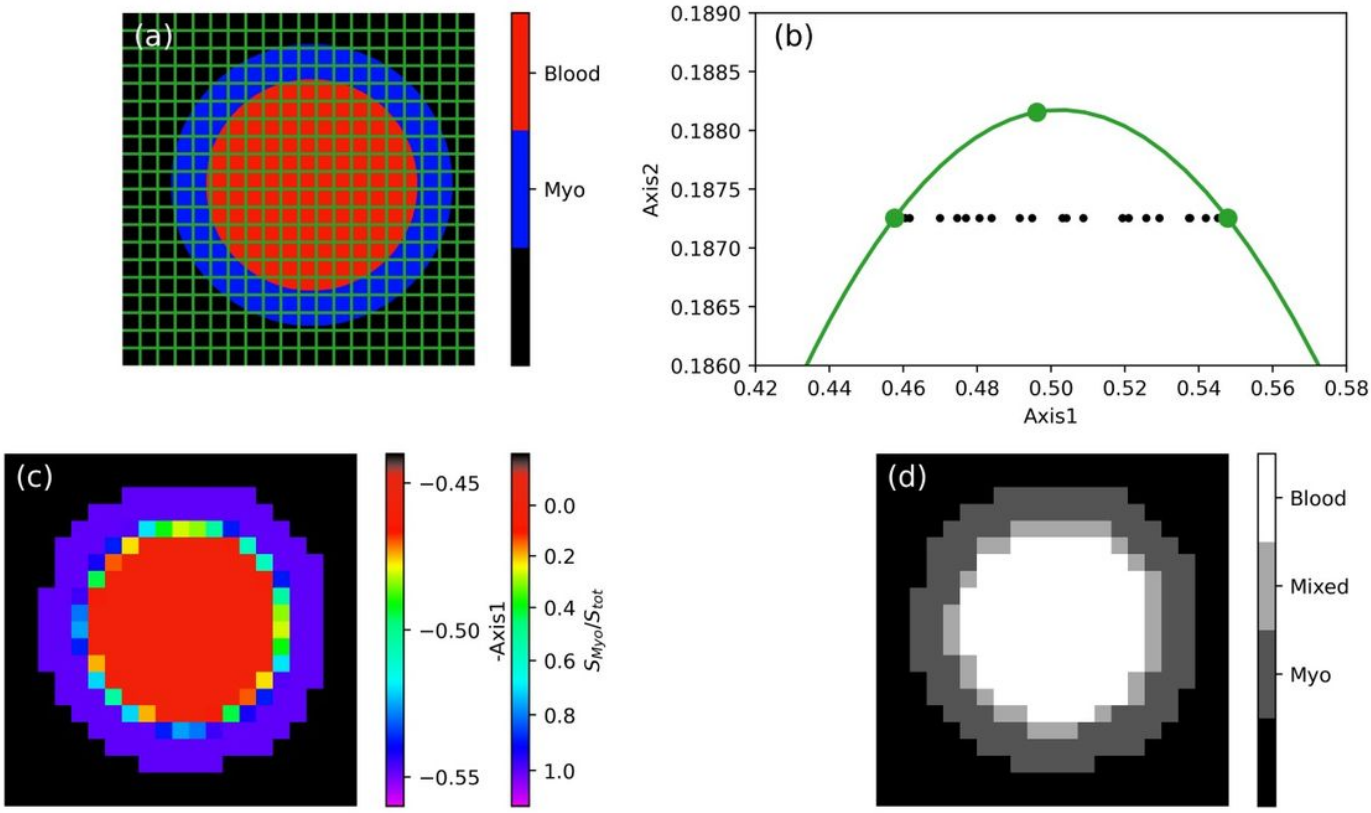

Figure 1

Phasor processing of T_1 qMRI data from a simulated heart phantom. (a) Sample architecture, indicating the used sampling grid, with the blood pool in red, and the myocardium in blue. The outside region in black corresponds to absence of MRI signal. (b) Full-harmonics phasor plot of the Inversion Recovery data simulated for the phantom in (a). In green, the mono-exponential reference curve and the dots referring to the three positions used for the full-harmonics projection with T_1 = 1.5, 1.75 and 2s.[18] (c) and (d) Image reconstructed from the phasor-space coordinates and its corresponding phasor-based segmentation, respectively.

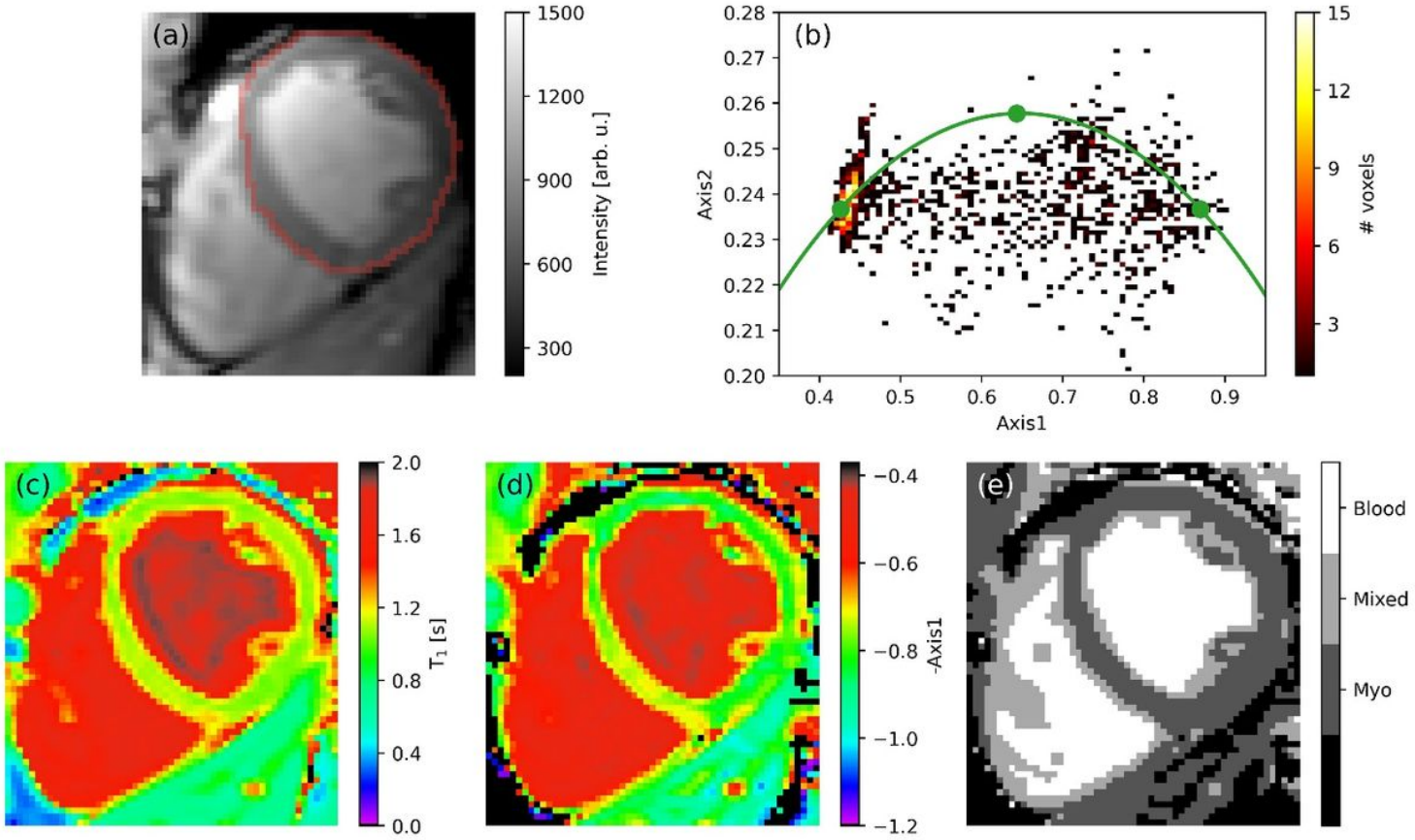

Figure 2

Phasor or fitting analysis of a ^{1}H T_1 qMRI dataset recorded on a healthy volunteer using a MOLLI pulse sequence. (a) Intensity map obtained from the first TI value of the MOLLI data. In red, the outline of the region selected for the phasor analysis is shown. (b) Full-harmonics phasor plot of the selected region. In green the mono-exponential reference curve is plotted, with the green dots referring to the three positions used for the full-harmonics projection.[18] (c) T_1 map obtained by single-exponential two-parameter fit. (d) Phasor-coordinate map derived from the x-axis coordinate of the phasor plot, where the phasor-coordinate colourmap has been inverted to match the colour scheme of the T_1 map in (c). (e) Map of the phasor-based segmentation.

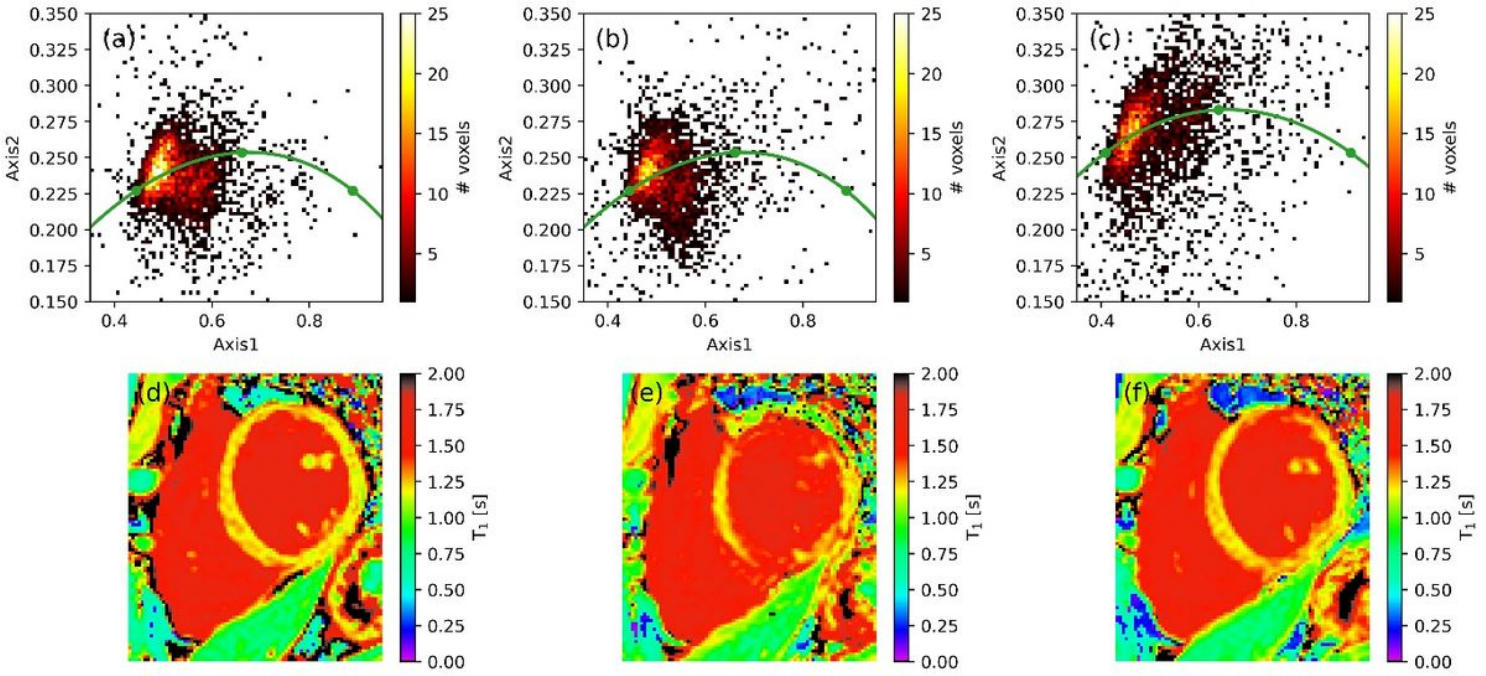

Figure 3

Effect of motion on phasor plots (top) and fitted T_1 maps (bottom) of a healthy volunteer. The columns refer to data either devoid of motion artifacts (left) or with added simulated motion using voxel shift (middle), and to data recorded during free breathing of the volunteer (right). The top row shows the full-harmonics phasor plot with the reference curve in green, while the bottom row shows the result of a single-exponential T_1 fit.

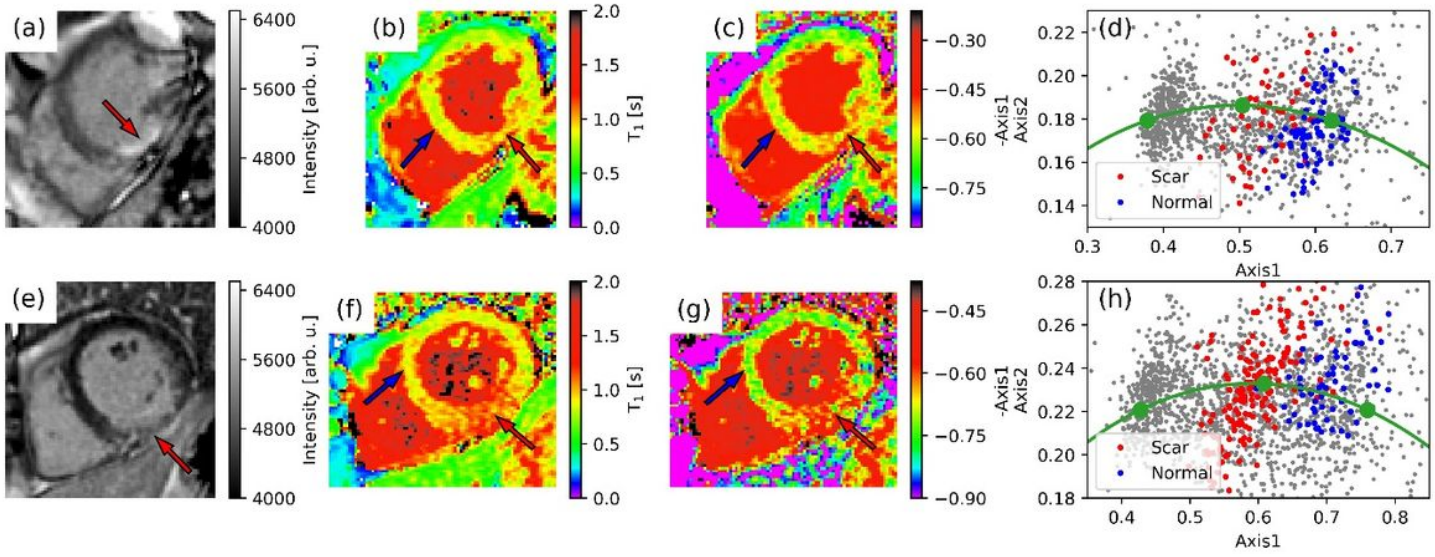

Figure 4

For two diseased individuals (a-d or e-h): phasor or fitting analysis of MOLLI data. (a,e) LGE images, with the scar indicated by the red arrow; (b,f) T_1 and (c,g) phasor-coordinates images; (d,h) phasor plots, with the voxels identified as scar muscle depicted in red, and a series of voxels of healthy normal myocardium

plotted in blue (see SI for the ROI's). The red and blue arrows in the phasor and T_1 maps indicate the regions where these voxels are taken from.

Supplementary Files

This is a list of supplementary files associated with this preprint. Click to download.

- MyocardiumSISciRep.docx